Predictions of turbulent secondary flows using the v^2-f model

By R. Pečnik AND G. Iaccarino

1. Motivation and objectives

Turbulent secondary flows, e.g., turbulent flows with streamwise mean vorticity (Bradshaw 1987) arise in many applications including ducts, jets in cross-flow, turbomachinery cooling passages, wall jets, etc. For statsitically stationary flows, streamwise vorticity can be generated by two essentially different mechanisms: deflection of existing mean vorticity or Reynolds stress imbalance. These are typically referred to as Prandtl's first and second kind of secondary flows.

The exact equation for the mean streamwise vorticity component is

$$v\frac{\partial \Omega_x}{\partial y} + w\frac{\partial \Omega_x}{\partial z} = \nu\nabla^2\Omega_x + \underbrace{\Omega_y\frac{\partial u}{\partial y} + \Omega_z\frac{\partial u}{\partial z}}_{A1} + \underbrace{\left(\frac{\partial^2}{\partial y^2} - \frac{\partial^2}{\partial z^2}\right)\left(-\overline{v'w'}\right)}_{A2} + \underbrace{\frac{\partial^2}{\partial y \partial z}\left(\overline{v'^2} - \overline{w'^2}\right)}_{A3}. \quad (1.1)$$

The terms in (A1) of Eq. 1.1 are responsible for generating the first kind, whereas the second kind is attributed to (A2) and (A3). Consider the *classic* fully developed, turbulent flow in a straight square duct then the last mentioned terms are responsible for the secondary motion. A symmetry argument (replace y with z) allows one to identify the term (A3) as the only possible source of streamwise vorticity. This results in two counter-rotating vortices at each of the duct corners that perturb the mean streamwise velocity. As a consequence, secondary flow convects momentum, vorticity and energy of the mean motion into the corner and then these quantities are transported away from the corner along the duct bi-sector walls (Gessner 1972).

Numerical simulations of secondary turbulent flows using eddy viscosity Reynolds Averaged Navier-Stokes (RANS) models fail to capture the streamwise vorticity generation mechanism. These models are based on the linear Boussinesq relationship between Reynolds stresses and mean velocity gradients (rate of strain). In addition, they rely on the assumption of normal stress isotropy and, therefore, the last term in Eq. 1.1 is identically zero. The poor predictive capabilities of eddy viscosity models in this application have been often cited as one of the major reasons for developing more sophisticated Reynolds stress closures.

The objective of this work is to introduce a simple extension of the stress-strain relationship that accounts for normal stress anisotropy. This leads to predictions of secondary turbulent flows in square and triangular cross-section ducts. It is the first time that this has been demonstrated in the framework of a purely linear eddy viscosity model.

There is no shortage of models that use an extension of the Boussinesq relationship. Non-linear eddy viscosity models, e.g., Gatski & Speziale (1993), and Algebraic Reynolds Stress Models (ARSM), e.g., Rodi (1976), have been shown to capture this flow with rea-

sonable accuracy. In the former, quadratic and cubic terms (in S_{ij} and Ω_{ij}, the symmetric and antisymmetric part of the velocity gradient tensor) are introduced, while in the latter, algebraic relationships are derived using equilibrium hypothesis for the Reynolds stresses (Girimaji 1997). On the other hand, the exact differential equations for the Reynolds stress components can be derived directly from the Navier-Stokes equations and form the basis of differential RSM; in this case, Eq. 1.1 is satisfied identically.

There are two fundamental issues in the development and use of these extended stress-strain models that have severely limited their wide use in the industrial community. The first is related to the need to introduce additional assumptions to formulate the closure. These tend to be more difficult to justify and involve high-order correlations that cannot be easily measured. The second issue is related to numerical stiffness and general lack of robustness observed in complex flows and caused by the strong non-linearity introduced. In addition, RSM-based models lead to greater computational cost than to simple eddy viscosity closures.

2. Modeling approach

We will consider the steady RANS equations for an incompressible fluid completed by the $v^2 - f$ turbulence model from Durbin (1991), Lien *et al.* (1998). As the model has gained an increasing popularity during the last years a variety of modifications have been introduced; hence, different versions are available. To avoid uncertainty about the model version used throughout this work, the equations and coefficients are reported in Appendix A. The equations are solved using a finite volume formulation on a multi-block structured grid; details of the algorithm used are given in Appendix B.

The starting point of the v^2-f model (as well as any other eddy viscosity model) is the Boussinesq relationship that links the mean velocity gradient to the turbulent stresses:

$$-\overline{u_i' u_j'} = 2\nu_t S_{ij} - \frac{2}{3} k \delta_{ij} \tag{2.1}$$

where ν_t is the eddy viscosity, k the turbulent kinetic energy, S_{ij} the symmetric part of the velocity gradient tensor and δ_{ij} the Kronecker delta. From this definition it is obvious that, although the underlying assumption states that the turbulence is anisotropic close to a wall (thus the introduction of a velocity scale v^2 independent of k), the overall effect on the mean flow is completely isotropic.

In the proposed work, we intend to follow an alternative route that is based on the maximum use of the information already computed in the framework of the v^2-f model. The objective is to modify Eq. 2.1 by keeping its linearity, although introducing a non-isotropic contribution. The Boussinesq relationship is substituted by:

$$-\overline{u_i' u_j'} \approx 2\nu_t S_{ij} - N_{ij}, \tag{2.2}$$

where the trace of N_{ij} has to preserve $N_{ij}\delta_{ij} = 2k$.

To derive the non-isotropic relationship for the normal Reynolds stresses we will first consider a fully developed turbulent channel flow, where the sole inhomogeneous direction is aligned with the $y-$axis. In this case the normal Reynolds stress component $\overline{v'^2}$ is directly approximated by the $v^2 - f$ model yielding $\overline{v'^2} = v^2$. The only turbulence anisotropy information available with the $v^2 - f$ model is the difference between v^2 and k and therefore we propose the following modification

$$N_{ij} = \frac{2}{3} k \delta_{ij} + \left(1 - \frac{3}{2}\frac{v^2}{k}\right)\left(\frac{1}{3}\delta_{ij} - n_i n_j\right) k, \tag{2.3}$$

where n_i is a unit vector defining the direction of anisotropy. The second term on the right-hand side of Eq. 2.3 fulfills the basic physical requirements, which are zero trace (solenoidal) and vanishing contribution in isotropic flow regions where $v^2 = 2/3k$. Furthermore the tensor notation ensures invariance under rotations and reflections of coordinate axes (Pope 2000). With the assumption of coincident directions of the inhomogeneity axis y and the direction of the anisotropy of the normal Reynolds stresses $\underline{n} = [0, 1, 0]$ Eq. 2.3 leads to

$$N_{ij} = \begin{bmatrix} k - \frac{1}{2}v^2 & 0 & 0 \\ 0 & v^2 & 0 \\ 0 & 0 & k - \frac{1}{2}v^2 \end{bmatrix}. \tag{2.4}$$

The next step in the model derivation is to remove the equality of the normal Reynolds stresses $\overline{u'^2}$ and $\overline{w'^2}$ in the plane parallel to the wall. This requires modeling the magnitude of $(\overline{v'^2} - \overline{w'^2})$, which is essential to accurately predict the secondary flow in the square duct, as shown by the term (A3) on the right-hand side of Eq. 1.1. We use the assumption that $\overline{w'^2}$ should scale with

$$\overline{w'^2} = f_d \frac{\overline{u'^2} + \overline{v'^2}}{2} \tag{2.5}$$

instead of $k - 1/2v^2$, which is a reasonable approximation for $y^+ > 50$. The function f_d in Eq. 2.5 was introduced to act as a damping function in near-wall regions to prevent an over-estimation of $\overline{w'^2}$ for $y^+ < 50$, and is given in the following subsection. The next task is to distinguish between the two components $\overline{u'^2}$ and $\overline{w'^2}$. In this initial formulation we take the normalized velocity vector u_i^* as a measure for the direction of the largest normal Reynolds stress component $\overline{u'^2}$. This component should remove the energy only from the component in the plane parallel to the wall. With the use of the velocity in Eq. 2.6 general invariance is no longer ensured (Girimaji 1997). This distinction between the two components is a first test to distribute the turbulent kinetic energy among them; further work is therefore still required. For the next step of model derivation, the ideas of Spalart & Shur (1997); Wallin & Johansson (2002) can be taken into account to obtain an appropriate formulation to ensure Galilean invariance.

The resulting form of the proposed Boussinesq extension with the preliminary assumptions can therefore be written as

$$N_{ij} = \frac{2}{3}k\delta_{ij} + C_{\mu_1}\left(\frac{\delta_{ij}}{3} - n_i n_j\right)k + C_{\mu_2}\left(2u_i^* u_j^* + n_i n_j - \delta_{ij}\right)k, \tag{2.6}$$

with

$$C_{\mu_1} = 1 - \frac{3}{2}\frac{v^2}{k}, \quad C_{\mu_2} = \frac{2 - f_d}{2 + f_d} - \frac{1}{2}\frac{v^2}{k}. \tag{2.7}$$

2.1. *Model details*

The model constants C_1 and C_2 have been introduced to allow for the possibility of turning off the extensions where isotropic turbulence arises, far away from walls. In certain situations within these regions, the $v^2 - f$ model predicts non-isotropic states leading to a non-zero expression for the term $\left(1 - 3v^2/2k\right)$. In these situations the parameters C_1 and C_2 can be set to zero. However, preliminary calculations for the test cases investigated in this brief showed that there was no need to apply the corrections and, therefore, $C_1 = 1.0$ and $C_2 = 1.0$ have been used.

The direction of anisotropy of the normal Reynolds stresses was obtained by means of

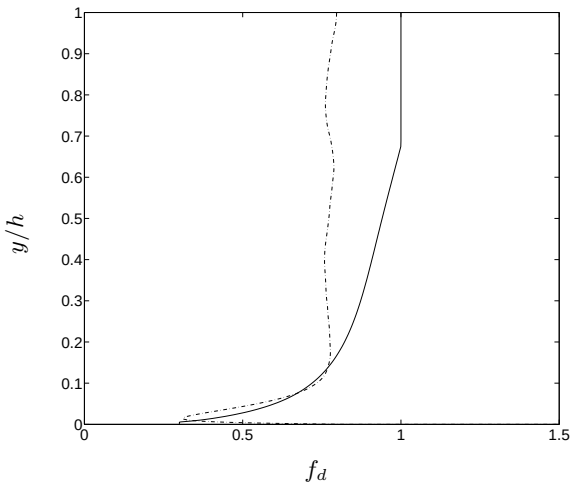

FIGURE 1. Damping function f_d for the channel at $Re_\tau = 590$: ——— using Eq. 2.10; —·— DNS by Moser *et al.* (1999).

a normalized gradient of a generic variable ϕ

$$n_i = \frac{\partial \phi}{\partial x_i} / \left| \nabla \phi \right|, \tag{2.8}$$

where ϕ was obtained by an elliptic relaxation equation given as

$$\nabla^2 \phi = C, \tag{2.9}$$

typically used to obtain smooth variations of the wall distance in complex geometries, Tucker (2000). Here $C = -1$, $\phi = 0$ at solid walls and $\partial\phi/\partial x_i = 0$ at open boundaries have been used.

The damping function f_d introduced in Eq. 2.5 has to ensure the correct asymptotic behavior of the components parallel to the wall, so that $\overline{u'^2} \propto y^2$ and $\overline{w'^2} \propto y^2$. As a first attempt this is achieved by setting the damping function to a constant value of $f_d = 0.3$ until $y^+ \approx 10$. Above this y^+ value the damping is modeled as a function of the ratio v^2/k. The resulting expression is given as

$$f_d = \min \left[\max \left(\left(\frac{3}{2} \frac{v^2}{k} \right)^{1/2}, 0.3 \right), 1.0 \right]. \tag{2.10}$$

Figure 1 shows a comparison between the f_d distributions obtained by Eq. 2.10 and the DNS for the fully developed turbulent channel flow at $Re_\tau = 590$. The modeled distribution deviates from the DNS for $h > 0.2$, as the DNS indicates a constant value of $f_d \approx 0.75$, unlike assumed by the approximation $\overline{w'^2} = 1/2(\overline{u'^2} + \overline{v'^2})$.

The final model results for the fully developed turbulent channel flow are displayed in Fig. 2. Recall that in the channel flow the normal stresses have no influence on the mean flow velocity, which makes this case appropriate for the model development. The determining quantity for the accurate prediction is hence only the turbulent shear stress $\overline{u'v'}$. Based on the v^2 distribution already given by the $v^2 - f$ model, the normal Reynolds stresses $\overline{u'^2}$ and $\overline{w'^2}$ are redistributed by the proposed model, with promising agreement with the DNS values.

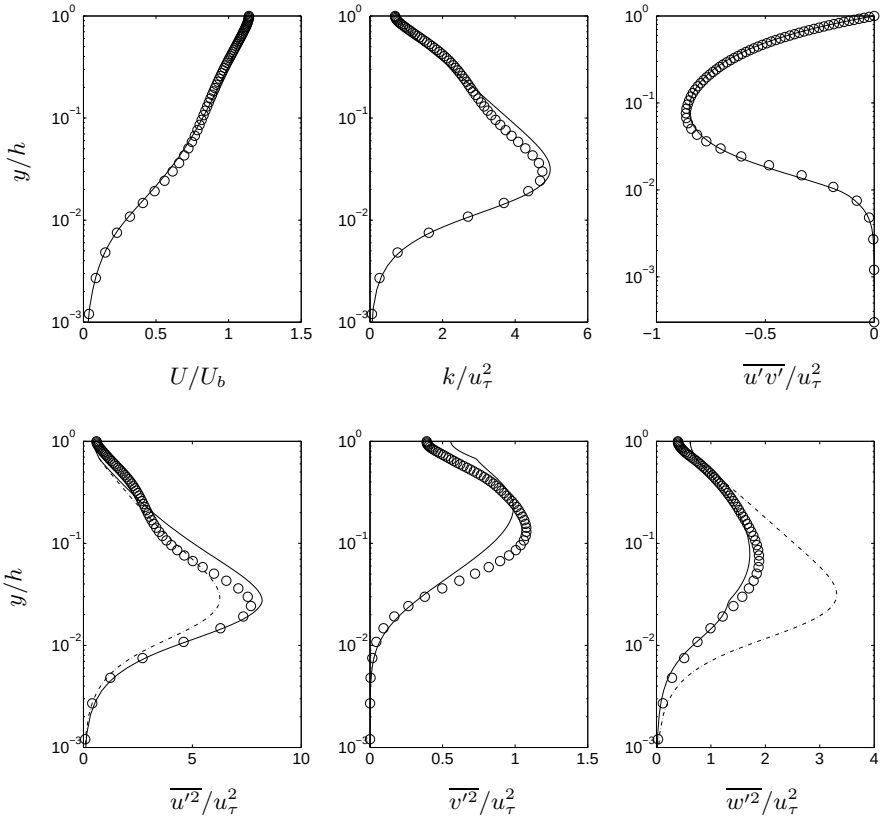

FIGURE 2. Channel flow at $Re_\tau = 590$: ——— $v^2 - f$ model with final model extension and f_d from Eq. 2.10 and —·— with $f_d = 1$; ∘ DNS by Moser *et al.* (1999).

3. Results

Two test cases, namely a square duct and an equilateral triangular duct have been investigated, both with fully developed turbulent flow to verify the proposed model extension for the ability to predict turbulence-driven secondary flow occurrence. In both cases computations have been performed as streamwise periodic flows with one cell in the flow direction. A source term $-dp/dx = u_\tau^2/h$ has been added to the momentum equation to account for the pressure gradient. For the square- and equilateral triangular duct calculations the wall shear stress τ_w was averaged over the wall cells.

3.1. *Fully developed turbulent straight square duct flow*

The vector plot in Fig. 3 shows the predicted secondary flowfield with the characteristic pair of counter-rotating streamwise vortices in the corner of the duct. The resultant distorted mean streamwise velocity is given by the contour plot in the same figure for one quarter of the square duct. A simple proof of the rotational invariance of the proposed model was obtained by rotating the square duct about 30°. Symmetric flow appears along the square ducts diagonal for the aligned (a) as well as for the rotated case (b).

A detailed comparison with the DNS data of Huser & Biringen (1993) is shown in Fig. 4

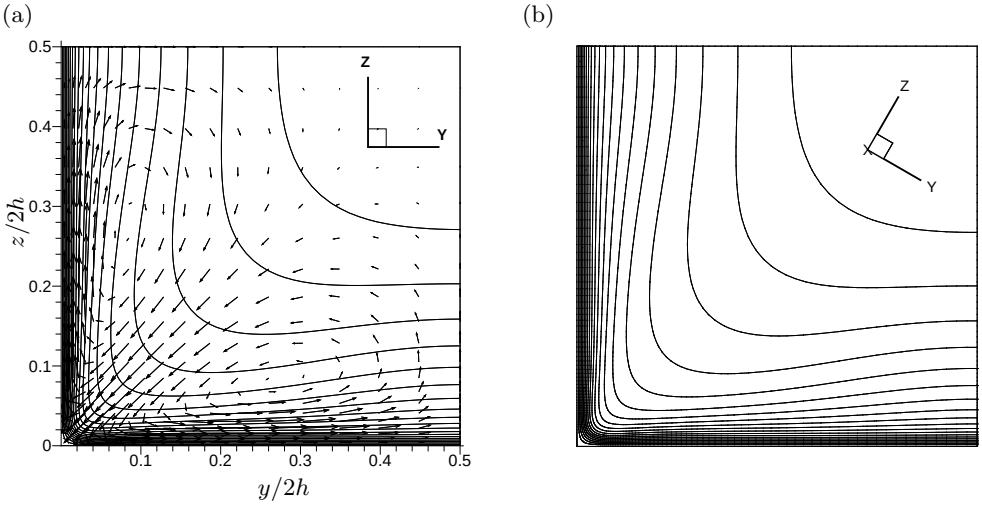

FIGURE 3. Square duct flow at $Re_\tau = 600$. Vectors: secondary flow; contours: mean streamwise velocity; (a) square duct aligned with Cartesian coordinate system; (b) 30° rotated.

for the primary (streamwise) U/U_b and secondary V/U_b flow components at different $y/2h$ locations. U_b stands for the bulk velocity, the Reynolds number based on the friction velocity is $Re_\tau = 2hu_\tau/\nu = 600$. It was found that the simple extension of the Boussinesq relationship is able to calculate the secondary flow component in very good agreement with the DNS. The magnitude, extent and location of the streamwise vortex match the DNS results very well, as indicated by the V/U_b distributions.

The secondary flow is induced by the anisotropy of the normal Reynolds stresses and therefore a detailed view of $\overline{u'^2}$, $\overline{v'^2}$ and $\overline{w'^2}$ normalized with u_τ is given in Fig. 5. The normal stresses are evaluated only from the proposed extension N_{ij}, although there is a contribution due to the strain from the Boussinesq relationship. For instance, the normal stress component is given by

$$-\overline{v'^2} = 2\nu_t S_{22} - N_{22}, \tag{3.1}$$

where S_{22} is non-zero because secondary flow appears in the duct; furthermore the contributions are negative as the trace for incompressible flows is $S_{ii} = 0$. To avoid the negative contribution to the normal Reynolds stress components, Eq. 2.6 can be revised with

$$-\overline{u_i' u_j'} = 2\nu_t S_{ij}\,(1 - \delta_{ij}) - N_{ij}, \tag{3.2}$$

but it has not yet been tested in the current investigation. The predictions of $\overline{u'^2}$ are in reasonable agreement with the DNS, whereas the stresses in the cross-flow plane are slightly over-predicted at the locations considered. However, the difference of these stresses is the only source for the secondary flow production, which is in good agreement with the DNS, leading to the superior agreement of the streamwise vortex.

Additionally the Reynolds shear stresses $\overline{u'v'}$ and $\overline{v'w'}$ are reported in Fig. 6. The turbulent stress $\overline{v'w'}$ acts only as a diffusion term for the streamwise vorticity (cf. 1.1 term (A2)) and has a lower impact on the flow development in the square duct. The over-predicted $\overline{v'w'}$ distribution is hence not reducing the performance of the model. The distribution of primary shear stress component $\overline{u'v'}$ is in reasonable agreement with the DNS.

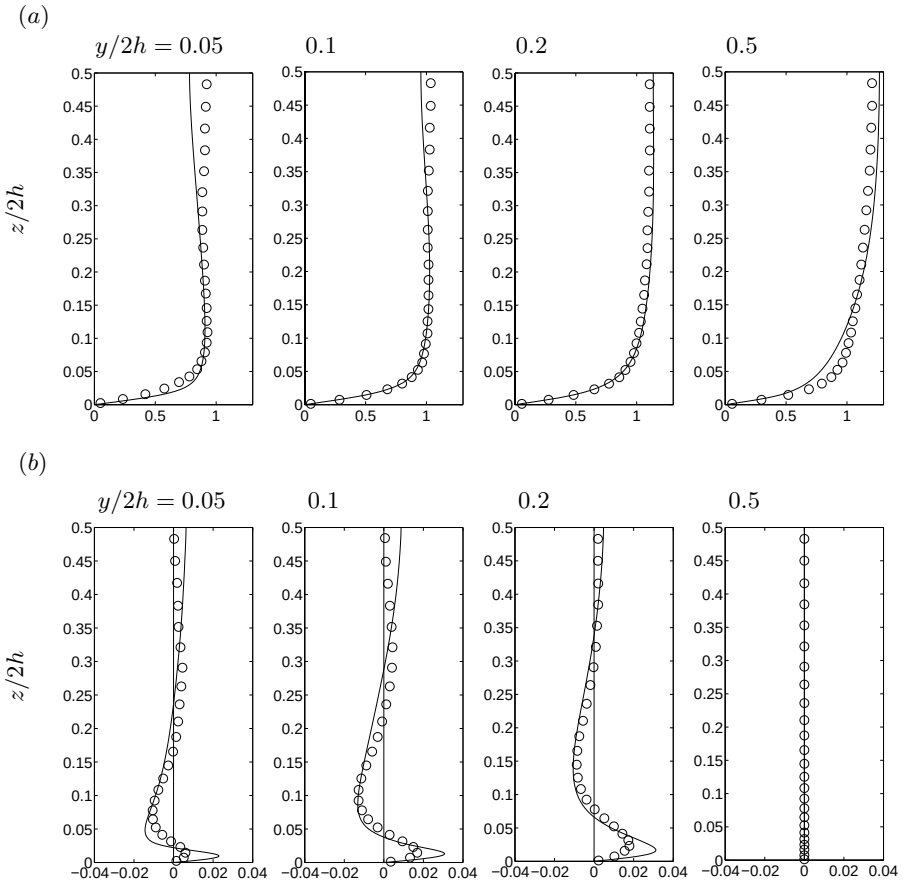

FIGURE 4. Square duct flow at $Re_\tau = 600$: (a) streamwise U/U_b (b) secondary V/U_b velocity component at different y locations; ——— present model extension; ○ DNS by Huser & Biringen (1993).

3.2. *Fully developed turbulent flow in an equilateral triangular duct*

Finally, a second model validation is given for a fully developed turbulent flow in a equilateral triangular duct. The model results are shown in Fig. 7 by means of a vector plot for one-third of the duct and by means of a contour plot of the streamwise velocity component. Symmetric flow along the altitude of the triangle appears with counter-rotating vortices in the corner, as it is for the square duct shown in Fig. 3, but with vortex centers closer to the corner. By comparing the secondary velocity V with measurements, a deviation is detected for the two distributions close to the mid of the duct with too weak secondary velocities, resulting in the displaced vortex centers.

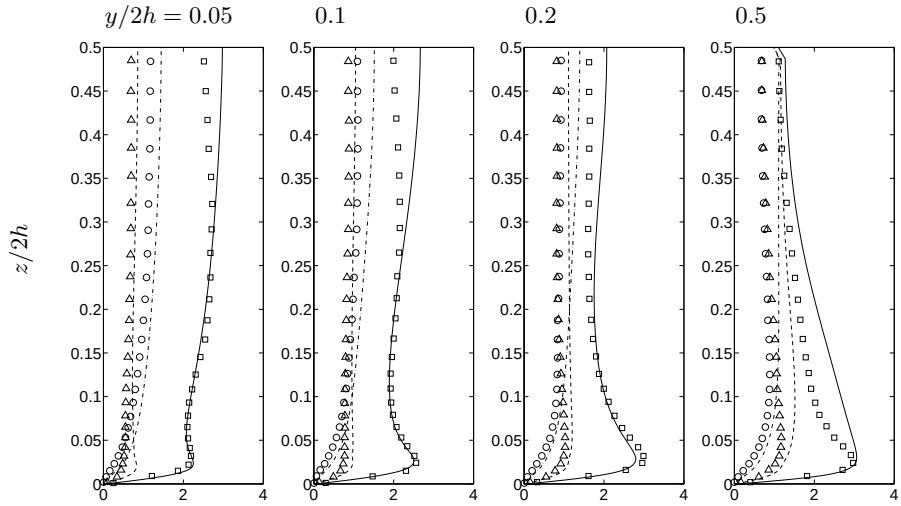

FIGURE 5. Square duct flow at $Re_\tau = 600$: ——— $\sqrt{\overline{u'^2}}/u_\tau$; —·— $\sqrt{\overline{v'^2}}/u_\tau$; - - - - $\sqrt{\overline{w'^2}}/u_\tau$ present model extension; symbols DNS by Huser & Biringen (1993).

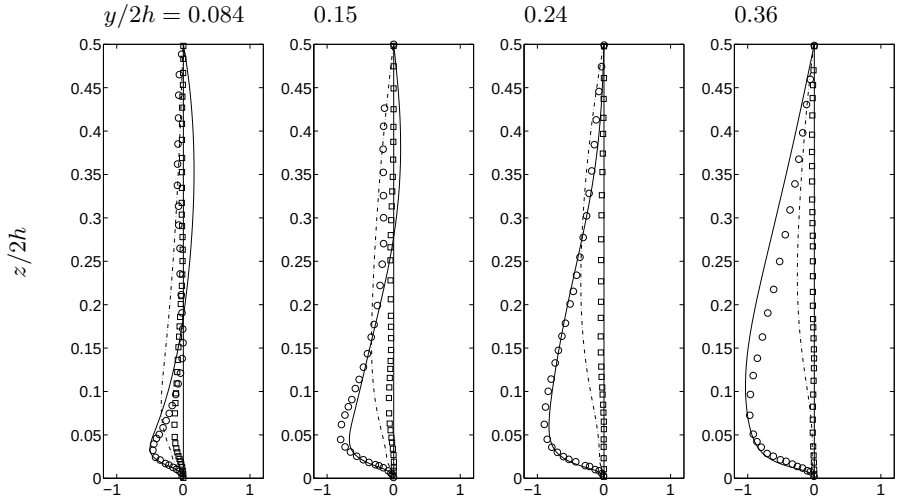

FIGURE 6. Square duct flow at $Re_\tau = 600$: ——— $\overline{u'v'}/u_\tau^2$; —·— $\overline{v'w'}/u_\tau^2$ present model extension; symbols DNS by Huser & Biringen (1993).

4. Conclusion and future work

A new stress-strain relationship for secondary turbulent flows was proposed in conjunction with the $v^2 - f$ turbulence model to mimic anisotropic normal Reynolds stress states. It has been proven that the proposed extension was able to accurately predict secondary flow appearance in fully developed flow on a straight square duct, where usually reasonable results could only be achieved by more complex modeling approaches, namely full Reynolds stress models or non-linear extensions to the Boussinesq relationship. This is apparently the first time that such an extension has been demonstrated in

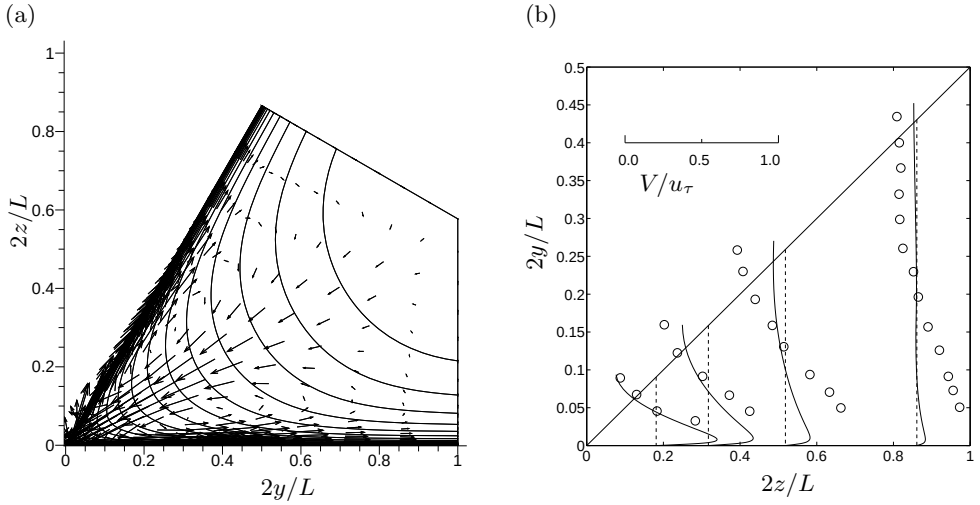

FIGURE 7. Equilateral triangular duct at $Re = 53000$. (a) Vectors: secondary flow of one-third section; (b) V/u_τ mean velocity component: ——— present model extension; ∘ experiments by Aly *et al.* (1977).

the framework of a purely linear eddy viscosity model. The distribution and magnitude of the secondary flow velocities were predicted with good agreement, compared to DNS data and measurements. However, the results for the equilateral triangular duct indicate that further development is needed. Compared to measurements, a displacement of the streamwise vortex toward the corner of the triangular duct was found. Hence some points need further work:

- the direction of anisotropy of the normal Reynolds stresses should be revised; on the one hand to avoid solving an additional elliptical relaxation equation, but also to obtain more reasonable results for the equilateral triangular duct previously mentioned. One possibility investigated is to use the gradient of f in the $v^2 - f$ model;
- the initial test with the velocity vector as a measure for the largest normal Reynolds stress component has to be replaced by a more reasonable Galilean invariant approach.

Appendix A

The transport equations for the turbulent kinetic energy k, the turbulent dissipation rate ε, the turbulent stress component normal to the stream lines v^2 and the elliptic

relaxation equation f for the source of v^2 are given by

$$\frac{\partial k}{\partial t} + u_j \frac{\partial k}{\partial x_j} - \frac{\partial}{\partial x_j}\left[(\nu + \nu_t)\frac{\partial k}{\partial x_j}\right] = P_k - \varepsilon \tag{4.1}$$

$$\frac{\partial \varepsilon}{\partial t} + u_j \frac{\partial \varepsilon}{\partial x_j} - \frac{\partial}{\partial x_j}\left[\left(\nu + \frac{\nu_t}{\sigma_\varepsilon}\right)\frac{\partial \varepsilon}{\partial x_j}\right] = \frac{C_{\varepsilon 1} P_k - C_{\varepsilon 2}\varepsilon}{T} \tag{4.2}$$

$$\frac{\partial v^2}{\partial t} + u_j \frac{\partial v^2}{\partial x_j} - \frac{\partial}{\partial x_j}\left[\left(\nu + \frac{\nu_t}{\sigma_{v^2}}\right)\frac{\partial v^2}{\partial x_j}\right] = fk - N\frac{v^2}{k}\varepsilon \tag{4.3}$$

$$L^2\nabla^2 f - f = \frac{C_1 - 1}{T}\left(\frac{v^2}{k} - \frac{2}{3}\right) - C_2\frac{2}{3}\frac{P_k}{k} + (N-1)\frac{1}{T}\frac{v^2}{k}. \tag{4.4}$$

The turbulent time scale T and length scale L are defined as

$$T = \max\left[\frac{k}{\varepsilon}, C_T\left(\frac{\nu}{\varepsilon}\right)^{1/2}\right],\ L = C_L \max\left[\frac{k^{3/2}}{\varepsilon}, C_\eta\left(\frac{\nu^3}{\varepsilon}\right)^{1/4}\right], \tag{4.5}$$

and the eddy viscosity is calculated with

$$\nu_t = C_\mu^v\, v^2\, T. \tag{4.6}$$

The model parameters are

$$\begin{aligned} C_{\varepsilon 1} &= 1.4(1 + 0.045\sqrt{v^2/k}) \\ C_\mu^v = 0.22,\ \ \sigma_{v^2} &= 1.0,\ \ C_{\varepsilon 2} = 1.92, \\ C_1 = 1.4,\ \ C_2 &= 0.45,\ \ \ C_T = 6.0 \\ \text{and for } N = 6:\ \ \sigma_\varepsilon &= 1.3,\ \ C_\eta = 70.0,\ \ C_L = 0.23\ , \end{aligned}$$

The boundary conditions at the wall w have been specified as

$$k_w = 0, \quad \varepsilon_w = 2\nu_1 k_1 / y_1^2, \quad v_w^2 = 0, \quad f_w = -(24 - 4N)\,\nu_1^2\, v_1^2/\varepsilon_1 y_1^4$$

where the index 1 represents the first wall cell.

Appendix B

The computations were performed using the Navier-Stokes code LINARS, which was developed at the Institute for Thermal Turbomachinery and Machine Dynamics at Graz University of Technology, Austria, given in Pecnik & Sanz (2007) and references therein. For the calculations presented herein the code was extended to solve the incompressible Reynolds-Averaged Navier-Stokes equations (RANS) by means of the artificial density approach, which can be written as

$$\frac{\partial p}{\partial t} + \beta\frac{\partial u_i}{\partial x_i} = 0 \tag{4.1}$$

$$\frac{\partial u_i}{\partial t} + \frac{\partial u_i u_j}{\partial x_j} = -\frac{1}{\rho}\frac{\partial p}{\partial x_i} + \frac{\partial}{\partial x_j}\left(2\nu S_{ij} - \overline{u_i' u_j'}\right), \tag{4.2}$$

where β is the artificial compressibility constant (Anderson *et al.* 1995). The code solves Eq. 4.2 in conservative form with a fully implicit time-marching finite-volume method on structured curvilinear grids. The inviscid (Euler) fluxes are discretized with upwind flux-difference splitting method. In order to achieve a high order of spatial accuracy, a

total variation diminishing (TVD) scheme with third-order interpolation was applied to get the state vector at each cell interface. The viscid flux vector at the cell interfaces is constructed with a second-order accurate central-differencing scheme, using Greens theorem.

Acknowledgments

The support by the Austrian Science Fund (FWF) with the Erwin Schröndiger Fellowship is greatfully acknowledged. The second author acknowledges early discussions with Dr. G. Kalitzin regarding the modified Boussinesq relationship.

REFERENCES

Aly, M.M., Trupp, A.C. & Gerrard, A.D. 1993 Measurements and prediction of fully developed turbulent flow in an equilateral triangular duct. *J. Fluid Mech.* **85**, 57–83.

Anderson, W. K., Rausch, R. D. & Bonhaus, D. L. 1995 Implicit/multigrid algorithms for incompressible turbulent flows on unstructured grids. *AIAA* **11**, 95–1704.

Bradshaw, P. 1987 Turbulent secondary flows. *Ann. Rev. Fluid Mech.* **19**, 53–74.

Durbin, P. A. 1991 Near-wall turbulence modeling without damping functions. *Theoret. Comput. Fluid Dyn.* **3**, 1–13.

Gatski, T. B. & Speziale, C. G. 1993 On explicit algebraic stress models for complex turbulent flows. *J. Fluid Mech.* **254**, 59–78.

Gessner, F. B. 1972 The origin of secondary flow in turbulent flow along a corner. *J. Fluid Mech.* **58**, 1–25.

Girimaji, S. S. 1997 A Galilean invariant explicit algebraic Reynolds stress model for turbulent curved flows. *Phys. Fluids.* **9**, 1067–1077.

Huser, A. & Biringen, S. 1993 Direct numerical simulation of turbulent flow in a square duct. *J. Fluid Mech.* **27**, 65–95.

Lien, F.S. & Kalitzin, G. and Durbin, P.A. 1998 RANS modeling for compressible and transitional flows. *Proceedings of the Summer Program 1998, Center for Turbulence Research, NASA-Ames/Stanford University*, 267–286.

Moser, R., Kim, J. & Mansour, N. 1999 Direct numerical simulation of turbulent channel flow up to $Re_\tau = 590$. *Phys. Fluids* **11**, 943–945.

Pecnik, R. & Sanz, W. 2007 Application of the turbulent potential model to heat transfer predictions on a turbine guide vane. *J. Turbomach.* **129**, 628–635.

Pope, B. S. 2000 Turbulent Flows. *Cambridge: Cambridge University Press.*

Rodi, W. 1976 A new algebraic relation for calculating the Reynolds stresses. *ZAMM* **56**, 219–221.

Spalart, P. & Shur, M. 1997 On the sensitization of turbulence models to rotation and curvature. *Aerospace Sci. Technol.* **1** No. 5, 297–302.

Tucker, P. G. 2000 Prediction of turbulent oscillatory flows in complex systems. *Int. J. Numer. Meth. Fluids.* **33**, 869–895.

Wallin, S. & Johansson, A.V. 2002 Modelling streamline curvature effects in. explicit algebraic Reynolds stress turbulence models. *Int. J. Heat and Fluid Flow.* **23**, 721–730.